A Study of Planetary Waves in the Southern Winter Troposphere and Stratosphere. Part II: Life Cycles

WILLIAM J. RANDEL* AND DUANE E. STEVENS

Department of Atmospheric Sciences, Colorado State University, Fort Collins, CO 80523

JOHN L. STANFORD

Department of Physics, Iowa State University, Ames, IA 50010

(Manuscript received 7 April 1986, in final form 29 September 1986)

ABSTRACT

Large-amplitude planetary waves in the southern winter stratosphere are observed to occur episodically, the result of episodic tropospheric forcing. This work is an observational study of the dynamics of the planetary waves, focusing on the evolution through a typical life cycle. Time lag correlations of wave amplitude with the Eliassen–Palm flux vector reveal the characteristic heat and momentum flux patterns associated with wave evolution. Energetic studies clearly show that the stratospheric waves can be understood in terms of a life cycle of vertical propagation from the troposphere, followed by decay from barotropic interactions with the zonal mean flow. Although usually of secondary importance, baroclinic decay of stratospheric wave energy is also observed, resulting from equatorward heat flux in the lower stratosphere. Good agreement in the energy balances discounts in situ instability in the stratosphere as a source of wave activity. An average or composite over several clearly propagating cases reveals the wave structure and evolution, and suggests a source of planetary wave activity in the upper troposphere.

1. Introduction

Enhanced planetary wave activity in the southern winter stratosphere is observed to occur episodically, with a characteristic time scale of 10–20 days between events. Part I of this study was a statistical analysis of the correlations of wave amplitude throughout the troposphere and stratosphere. It was observed that stratospheric wave maxima could be traced into the troposphere with a time lag of several days, indicative of vertical propagation. Additionally, the structure of the planetary waves in the meridional plane was studied, and remarkable in- and out-of-phase coherent fluctuations were revealed. A high degree of reproducibility in the statistics over two winters suggested these to be fundamental signatures of the planetary waves.

The objective of Part II is to detail the dynamics of the planetary waves throughout a typical life cycle, with the aid of wave–mean flow interaction diagnostics. A time-lag cross-correlation analysis of wave amplitude with the Eliassen–Palm flux vector reveals the characteristic heat and momentum flux patterns associated with wave evolution. An energetic analysis based on the transformed Eulerian mean formalism of Plumb (1983) clearly shows that the stratospheric waves undergo a life cycle of vertical propagation from the troposphere, followed by decay from barotropic interactions with the polar night jet. An average or composite over several vertically propagating cases provides a clear look at the troposphere–stratosphere interaction, and suggests a source of planetary wave activity in the upper troposphere. Time changes in the quasi-geostrophic wave activity are calculated and found to be well correlated with the observed wave driving over much of the midlatitude stratosphere.

Finally, we discuss the nature of the tropospheric forcing of the planetary waves in light of these observations and those from Part I.

2. Data analyses and quality

a. Analyses

The data used here are wind and hydrostatic temperature fields derived from the National Meteorological Center (NMC—100 mb and below) and Climate Analysis center (CAC—70 mb and above) geopotential height data, as described in Part I. Evaluation of the wind fields is discussed below. Gradient wind balance is used to evaluate zonal mean winds. Data for two 120-day southern winters (1 June–28 September 1983 and 1984) were analyzed. Because zonal waves 1 and

* Present address: National Center for Atmospheric Research, Boulder, CO 80307. NCAR is sponsored by the National Science Foundation.

2 dominate the wave variance in the stratosphere (see Part I), those waves are primarily analyzed.

Many of the results presented here are based on wave–mean flow interaction diagnostics, predominantly Eliassen–Palm (EP) flux diagrams.

We use the quasi-geostrophically scaled form of the EP flux:

$$\mathbf{F} = \begin{pmatrix} F_\phi \\ F_z \end{pmatrix} = e^{-z/H} a \cos\phi \begin{pmatrix} -\overline{u'v'} \\ \frac{R}{H} f \frac{\overline{v'T'}}{N^2} \end{pmatrix}. \quad (1)$$

where overbars and primes represent zonal means and deviations therefrom, and notation is standard.

Because we desire to view the EP vectors throughout the stratosphere, the vectors are scaled by $e^{+z/2H}$. Additionally, F_z is scaled by a deformation factor of (N/f), such that the two components of F are plotted isotropically in the latitude–height plane (Palmer, 1982). A representative value of N/f in the stratosphere is 150; the EP vectors are thus drawn such that the reference arrow in the upper right-hand corner of each diagram represents $(ae^{z/2H})$ times 15 $m^2\ s^{-2}$ of F_ϕ and 0.1 $m^2\ s^{-2}$ of F_z.

The transformed Eulerian mean (TEM) zonal mean momentum equation is:

$$\frac{\partial \bar{u}}{\partial t} = f\overline{v^*} + \mathrm{DF}, \quad (2)$$

where

$$\mathrm{DF} = \left[\frac{1}{a\cos\phi}\frac{\partial}{\partial\phi}(F_\phi \cos\phi) + \frac{\partial F_z}{\partial z}\right] \Big/ (e^{-z/H} a \cos\phi) \quad (3)$$

is proportional to the EP flux divergence, also called the wave driving, and $\overline{v^*}$ is the meridional residual circulation. Contours of the wave-driving term DF are plotted in the EP flux diagrams, with units of m s^{-1} per day.

The energy calculations here are based on the TEM formalism of Plumb (1983). The wave–mean flow energy exchange term in the TEM formalism is given by

$$\frac{\partial E'}{\partial t} = -\int \cos\phi d\phi \int dz e^{-z/H} \bar{u}(\phi, z)\mathrm{DF}(\phi, z) \quad (4)$$

where E' is the total wave energy (available potential plus kinetic), $\bar{u}$ is the zonal mean wind, and DF is defined in Eq. (3). The limits of integration for the stratospheric calculations are 25°–75°S and 100–2 mb.

As discussed in Palmer (1982), linear waves on a steady zonal flow satisfy the following local conservation equation:

$$\frac{\partial A}{\partial t} + \mathrm{DF} = S, \quad (5)$$

where S is a nonconservative term, DF is defined above, and A is the (modified) measure of local quasi-geostrophic wave activity:

$$A = \frac{1}{2}\overline{q'^2}/\bar{q}_y. \quad (6)$$

Regions of positive DF correspond to a local decrease of A; more wave activity is leaving than entering such a region, which is therefore referred to as a source of wave activity. Here q' is the (modified) wave potential vorticity (Palmer, 1982):

$$q' = \frac{1}{a}\left[\frac{1}{\cos\phi}\frac{\partial v'}{\partial\lambda} - \frac{\sin\phi}{\cos\phi}\frac{\partial}{\partial\phi}\left(\frac{\cos\phi}{\sin\phi}u'\right)\right] + 2\Omega \sin\phi e^{z/H}\frac{\partial}{\partial z}\left(e^{-z/H}\frac{1}{N^2}\frac{\partial\Phi'}{\partial z}\right),$$

with Φ' the geopotential height, and $\bar{q}_y$ the zonal mean potential vorticity gradient:

$$\bar{q}_y = \frac{2\Omega}{a}\cos\phi - \frac{1}{a^2}\frac{\partial}{\partial\phi}\left[\frac{1}{\cos\phi}\frac{\partial}{\partial\phi}(\bar{u}\cos\phi)\right] - (2\Omega\sin\phi)^2 e^{z/H}\frac{\partial}{\partial z}\left(e^{-z/H}\frac{1}{N^2}\frac{\partial\bar{u}}{\partial z}\right).$$

Because of the high number of derivatives involved in Eq. (6), some spatial smoothing was used on the geopotential fields before q' and $\bar{q}_y$ were calculated. In all of the above calculations a static stability (N^2) dependent on latitude and height was used, based on the seasonal and zonal mean temperature structure.

Horizontal wind fields were evaluated by linearizing the zonal and meridional momentum equations about the zonally averaged flow, and neglecting the local time tendencies with respect to advection by the zonal mean wind. This results in the following two coupled linear equations:

$$\frac{\bar{u}}{a\cos\phi}\frac{\partial u'}{\partial\lambda} - \hat{f}v' = -\frac{1}{a\cos\phi}\frac{\partial\Phi'}{\partial\lambda} \quad (7a)$$

$$\frac{\bar{u}}{a\cos\phi}\frac{\partial v'}{\partial\lambda} + \hat{f}u' = -\frac{1}{a}\frac{\partial\Phi'}{\partial\phi}, \quad (7b)$$

where

$$\hat{f} = \left[2\Omega\sin\phi - \frac{1}{a\cos\phi}\frac{\partial}{\partial\phi}(\bar{u}\cos\phi)\right]$$

$$\tilde{f} = \left(2\Omega\sin\phi + \frac{2\bar{u}}{a}\tan\phi\right).$$

These equations are solved for each zonal wavenumber to evaluate the spectral components of u' and v'; we call the resulting wind estimates "linear" winds. Note that these equations become singular at wavenumber k as

$$\delta \equiv \frac{(\bar{u}K/a\cos\phi)^2}{(\hat{f}\tilde{f})} \to 1.$$

This is typically observed for zonal wavenumbers greater than 4 in the core of the polar night jet. For

the data presented here, geostrophic winds were substituted for the linear winds if $\delta > 0.5$ (the results are not sensitive to this exact value).

This analysis was used here because recent studies (numerical model results of Robinson, 1986; Boville, 1987; and observational analyses of Randel, 1987) have shown that geostrophically evaluated winds result in substantial overestimates of the poleward momentum flux in the stratosphere, due to the neglect of centrifugal accelerations in the geostrophic approximations. Poleward heat flux estimates are not strongly affected. The resulting geostrophic wind EP flux divergence values in the high latitude stratosphere are systematically overestimated, due primarily to the momentum flux errors. Extensive comparisons with numerical model simulations and observational data (Randel, 1987) show that the use of linear wind fluxes substantially alleviates this problem.

b. *Data quality*

The quality of hemispheric meteorological analyses is always suspect in the Southern Hemisphere, and a particularly sensitive and notoriously poor calculation is that of poleward heat flux (i.e., van Loon, 1980). Because the heat flux by planetary waves is of central importance in this study, we test the data quality used here by comparison with that analyzed by the European Centre for Medium Range Weather Forecasts (ECMWF). The latest year of ECMWF data available to us was 1982, and we compare the June–July–August 1982 values, noting that there is little difference in the NMC/CAC derived fields between this winter and the 1983/84 winters studied throughout the rest of this paper. Of particular importance to the results discussed here is the vertical structure and time dependence of the k = 1–2 heat flux in middle to high latitudes throughout the troposphere. Note that the NMC/CAC heat flux values are based on linear winds (which are nearly geostrophic in the troposphere), while the ECMWF values are based on the actual analyzed wind fields.

Figures 1a, b display the time mean (June–July–August) heat flux for k = 1–2 based on NMC/CAC analyses (only data from 1000–30 mb is plotted here) and ECMWF analyses (which were available for 1000–100 mb). Both analyses show maxima of comparable magnitudes in the lower troposphere near 30°–40°S and 55°–70°S, and also above 300 mb in the 45°–65°S latitude band. Two major differences are found: 1) In the low latitude upper troposphere, the ECMWF data show a poleward maximum not found in the NMC/CAC data, and 2) in latitudes poleward of 70°S throughout 1000–100 mb, where the NMC/CAC analyses show an unrealistic vertical structure and the two data sets are quite different. Problems in this region can arise from the Antarctic topography, the contamination of satellite temperature retrievals by persistent cloud cover, and other factors. However, the 40°–70°S latitude band is of more importance to the present study, and overall the agreement in the time mean in this region is quite encouraging.

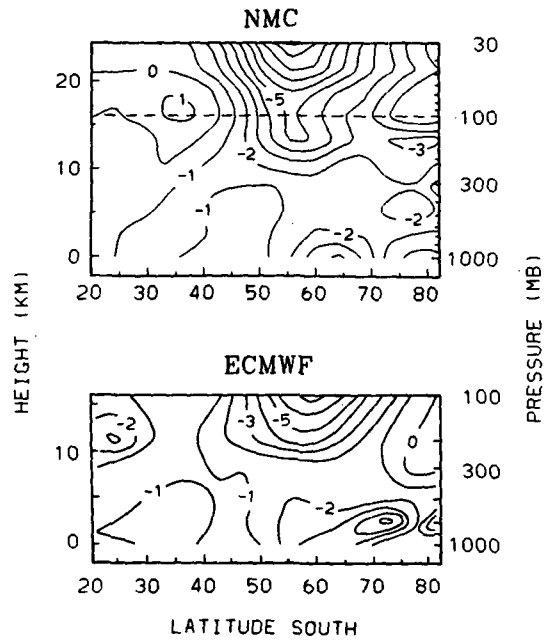

FIG. 1. Meridional cross sections of the time average (June–July–August 1982) zonal wavenumber 1–2 northward heat flux (°k-m s^{-1}) throughout the troposphere of the Southern Hemisphere, based on data produced by NMC/CAC (top) and ECMWF (bottom).

The time dependence of the two analyses in the 55°–65°S latitude band throughout the troposphere is displayed in Fig. 2, which shows time series from both data sets at 100, 200, 300, 500, and 700 mb. Good agreement is observed at all levels, promoting confidence in the fidelity of the NMC analyses in the SH troposphere, at least for planetary scale features in midlatitudes.

3. Results

a. *Wave amplitude–EP flux correlations*

Because the observed geopotential height fluctuations in the stratosphere occur episodically (for example, see Fig. 3 of Part I), cross-correlation analysis is well suited to study the associations of wave amplitude and EP flux (which is proportional to the wave group velocity). Correlations of wave amplitude with the two components of **F** (F_ϕ and F_z) are considered separately.

Figure 3 shows meridional cross sections of the correlation coefficient between zonal wavenumber 1 (k = 1) wave amplitude in the middle stratosphere (10 mb, 55°S) with k = 1 F_z at all latitudes and pressures, for time lags of −6, −4, −2 and 0 days (F_z leading

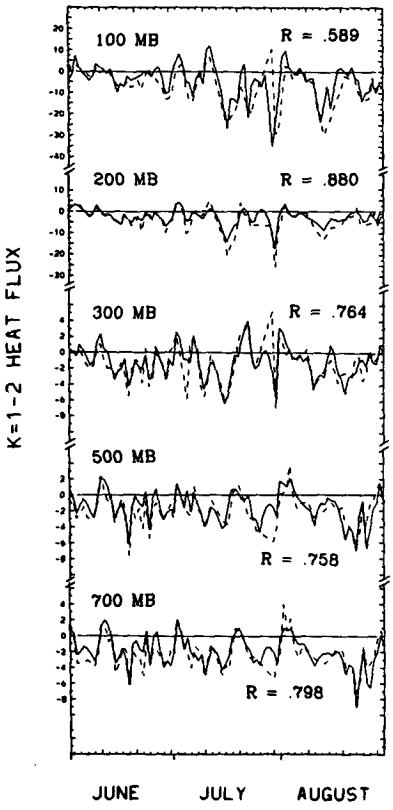

FIG. 2. Time series of the zonal wavenumber 1–2 northward heat flux (°k-m s^{-1}) averaged over 55°–65°S at 100, 200, 300, 500 and 700 mb, based on data from NMC/CAC (solid) and ECMWF (dashed). The correlation coefficient (R) is also shown for each level.

upper-level wave amplitude). The strongest correlations decrease in altitude as the time lag is increased, i.e., the vertical group velocity maxima occur prior to and at lower levels than the wave amplitude maxima. The correlations fall off sharply below the lower stratosphere. In fact, the position and meridional slope of the tropopause is echoed rather sharply in these cross-correlation maps: vertical group velocity (poleward heat flux) is most coherent *above* the tropopause prior to stratospheric wave amplitude maxima. Note this is probably not an artifact of the data processing, because the upper and lower analyses are joined at 100 mb; the observed patterns are smooth across this level. The location of the strongest correlations suggest that upward propagation occurs primarily over the 45°–60°S latitude region. The meridional scale of the cross-correlation patterns is narrow in the lower stratosphere, as compared with broader patterns above roughly 50 mb.

Figure 4 shows similar calculations based on heat flux values from the NMC and ECMWF data for 1982, as discussed in section 2. The agreement between these data confirms that the drop of correlation across the tropopause region is not an artifact of spurious SH tropospheric analyses at NMC, but rather a genuine feature.

To delineate the time dependence of the wave 1 correlation patterns more clearly, Fig. 5a is a height–time lag section of these correlations at 55°S, with reference point at 10 mb (the values at −6, −4, −2 and 0 days correspond to vertical sections at 55°S in Fig. 1). The strongest values are observed in the low-to-middle stratosphere for −2 to −7 days lag; the 1984 correlations show the strongest values for −2 to −5 days. This time scale agrees with the approximate 3–5 day time lag observed in Part I for strongest $k = 1$ stratosphere-troposphere coherence.

Figure 5b shows a similar vertical section, but for a 300 mb $k = 1$ amplitude reference position. Here the strongest correlations are found at +1 to +3 days lag, again only *above* the tropopause level; near-identical

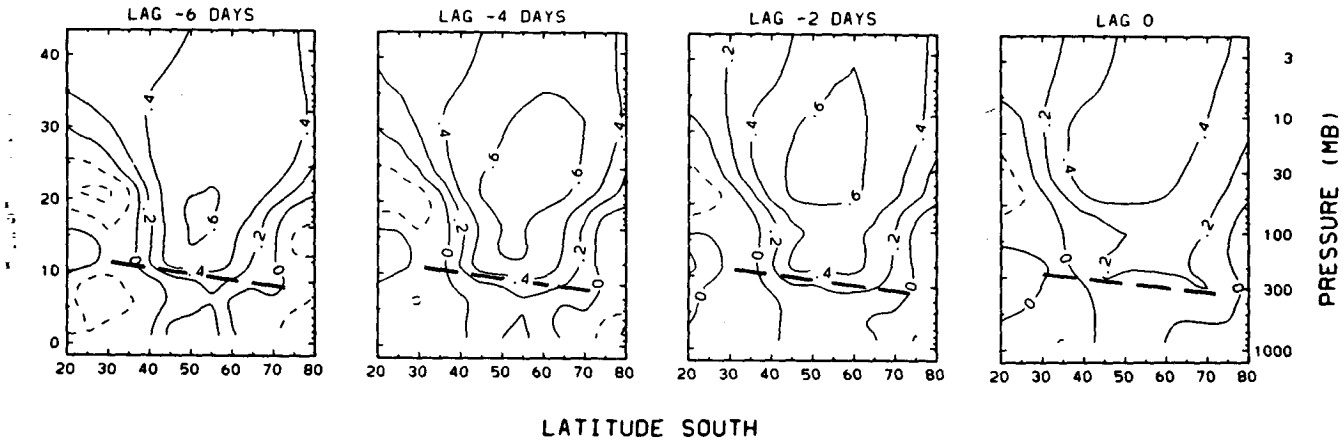

FIG. 3. Meridional cross sections of the cross-correlation coefficient between wave 1 amplitude at 10 mb, 55°S and wave 1 poleward heat flux at each latitude and pressure, for time lags of −6 to 0 days (heat flux leading wave amplitude). Note the sharp dropoff of correlation across the region of the tropopause, indicated by the heavy dashed line.

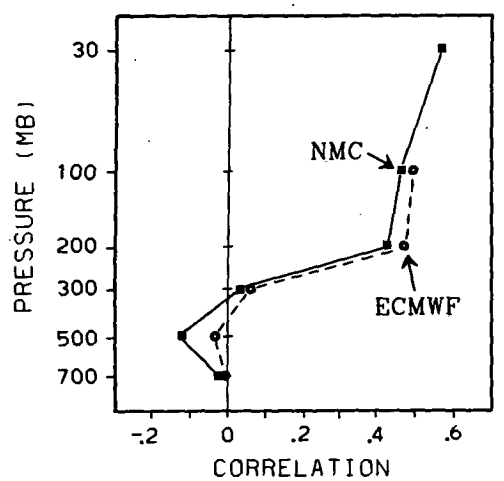

FIG. 4. Correlation coefficient between the square root of the variance of zonal waves 1–2 at 10 mb, 55°S and poleward heat flux averaged over 55–65°S at the indicated pressure levels, for a lag of −2 days (heat flux leading wave amplitude), over June–July–August 1982. Shown are results based on heat flux data from NMC/CAC (solid) and ECMWF (dashed).

behavior is observed in the 1984 statistics. The 300 mb $k = 1$ maxima are not most strongly correlated with lower tropospheric poleward heat flux (as would be observed in a baroclinically growing planetary wave); rather, the strongest correlations are observed above the tropopause several days later!

Figure 6 shows meridional cross sections as in Fig. 1, but for wave 2 statistics at −3, −2, −1 and 0 days time lag. Patterns very similar to those in Fig. 3 are observed, with sharp falloff of correlation across the tropopause. Note the time scales here are approximately one-half those for wave 1; similar behavior was found for the amplitude cross correlations in Part I. Figure 7a is a height–time lag section at 55°S, with reference at 10 mb, highlighting the time variations seen in Fig. 6. An approximate 1–2 day time lag is observed between lower-to-middle stratosphere F_z and 10 mb $k = 2$ amplitude. Figure 7b is a similar plot using a 300 mb reference; here poleward heat flux below 500 mb is observed to precede the 300 mb $k = 2$ amplitude maxima (although a similar plot for 1984 shows the strongest correlations above 250 mb).

For comparison, Fig. 8 shows a similar height–time lag cross section for wave 4, which is predominantly a tropospheric mode. Strong correlations with lower tropospheric poleward heat flux are found 0–1 days prior to 300 mb wave amplitude maxima, a clear signature of the baroclinically forced nature of those waves.

Part I of this study showed that wave 1 and wave 2 height fluctuations exhibit distinct vertical structures, with wave 1 being out-of-phase between the middle stratosphere and middle troposphere, while wave 2 is nearly in phase. Here we observe that wave amplitude/heat flux correlations show very similar characteristics for both wave 1 and wave 2, although with different time scales. These correlations show a common dynamical signature; the picture that arises statistically is of long-wave excitation in the troposphere, followed by strong vertical group velocity above the tropopause and subsequent wave amplitude growth in the stratosphere.

Cross correlations of wave amplitude with F_ϕ indicate that wave amplitude maxima are most strongly correlated with equatorward F_ϕ (poleward momentum flux) in low to middle latitudes in the middle-to-upper stratosphere near zero time lag. Very similar signatures are found for the wave 1 and wave 2 statistics. Little consistency is observed of the momentum flux correlations in the troposphere, suggesting that momentum flux is not a decisive factor in the development of the waves there.

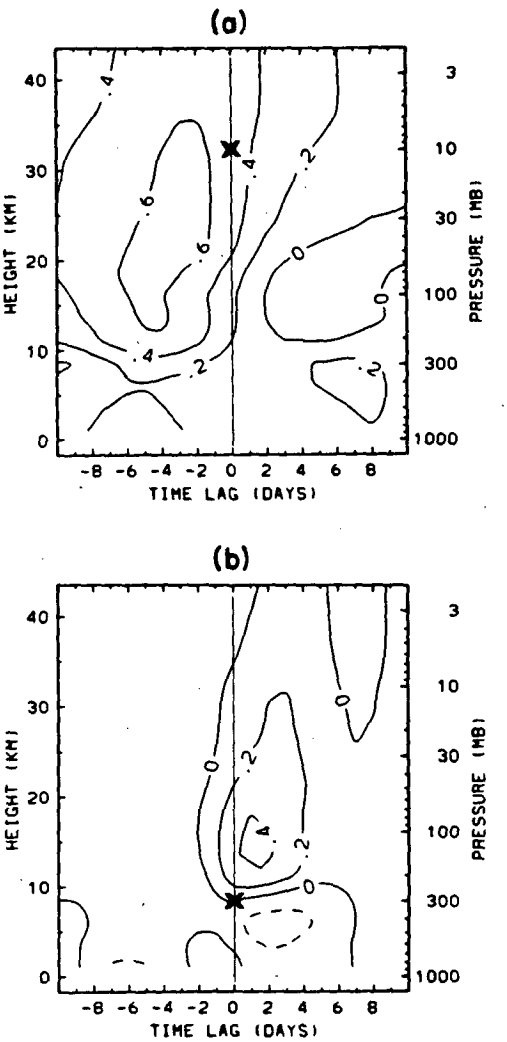

FIG. 5. (a) Height–time lag section at 55°S of the cross-correlation coefficient between $k = 1$ amplitude at 10 mb, 55°S, and $k = 1$ poleward heat flux at all pressure levels. Wave amplitude reference position at 10 mb is marked with an '×.' (b) As in (a) but for a wave amplitude reference position at 300 mb, 55°S.

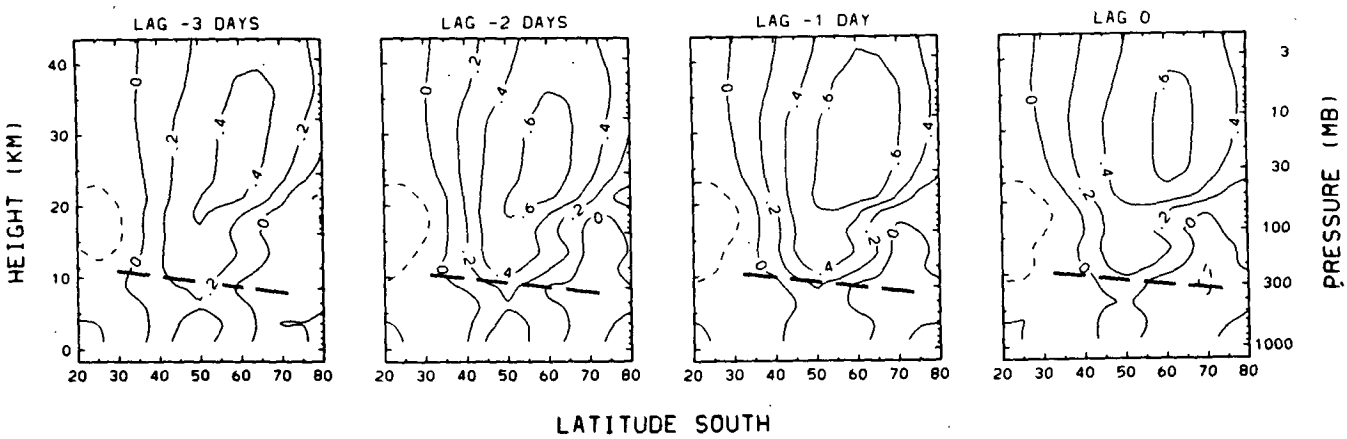

FIG. 6. As in Fig. 1 but for wave 2 cross-correlations at time lags of −3 to 0 days. Note the similar patterns to the wave 1 correlations, with the time scales cut roughly in half.

b. Wave–mean flow interactions and energetics

The life cycle characteristics of the stratospheric waves are clearly illustrated by consideration of wave–mean flow interaction diagnostics. Although previously the dispersive nature of the wave 1 and wave 2 components have been illustrated, much of the rest of the discussion here will consider the combined effects of waves 1 and 2. This choice is based on (i) the desire to study the total wave structure in the stratosphere (where k = 1–2 contribute greater than 90% of the variance), (ii) the observation that episodes of increased wave activity often have contributions from both wave 1 and wave 2, and (iii) the fact that the wave–mean flow interaction characteristics are similar for both components. Although wave-wave interactions clearly occur, they are not the subject of this study.

We first consider the zonally-averaged energy budget, based on Eq. (4). Figures 9a–b show the total available potential plus kinetic energy in the stratospheric (100–2 mb) zonal mean flow and for waves 1–2, for both 1983 and 1984. The observed wave energy changes are generally compensated by opposing zonal mean energy changes, showing that wave–mean flow energy exchange is a valid concept here.

Figures 10a–b show the observed time rate of change of stratosphere k = 1–2 energy for each year (the time derivative of the lower curves in Figs. 9a–b), along with that calculated from the wave–mean flow interaction term [Eq. (4)]. Good agreement between these terms is observed, although calculated energy changes are usually somewhat larger than those observed, particularly during periods of wave energy loss. To the degree that the curves in Figs. 10a–b agree, the wave energy changes can be understood both qualitatively and quantitatively in terms of the wave-induced mean flow interactions. This provides a powerful diagnostic of the growth and decay mechanisms.

Figures 11a–b display the separate baroclinic and barotropic contributions to the mean flow interaction term for k = 1–2 (i.e., the separate contributions of F_z and F_ϕ to DF in Eq. 4), along with the k = 1–2 energy for reference for each year. Peaks in wave energy are clearly preceded by peaks in the baroclinic interaction term, confirming that vertical propagation (associated with the poleward heat flux) is the physical process responsible for the observed wave growth. Note that these diagnostics say nothing about the cause of the observed heat flux; baroclinic instability is not indicated by the observed baroclinic wave–mean flow interactions.

Barotropic interactions in Fig. 11a are observed to be negative, indicative of a loss of energy from the waves to the mean flow. The maxima in barotropic decay occur in tandem with wave energy maxima, subsequent to the baroclinic growth maxima. The overall picture that arises from this energetic analysis is one of a well-defined planetary wave life cycle in the stratosphere, with distinctive wave growth and decay processes.

Note that baroclinic *decay* (negative values of curves "BC") is often observed subsequent to wave energy peaks in Figs. 11a–b. Although usually not as large as the barotropic decay maxima, some cases of wave decay are dominated by this mechanism (see Fig. 11a near 20 September and Fig. 11b near 12 September). These baroclinic decay periods are the result of strong *equatorward* heat flux throughout the lower stratosphere as the waves decay. A striking example is shown in Fig. 12, where the EP flux vectors averaged over 19–21 September 1983 are shown; note the downward pointing arrows throughout the stratosphere. Some hint of this behavior is also observed in the heat flux correlation patterns; note the negative correlation in the lower stratosphere at positive time lags in Figs. 5a and 7a. The downward pointing EP flux vectors in the lower stratosphere suggest *downward* propagation of the wave energy during these periods, and indeed some hint of

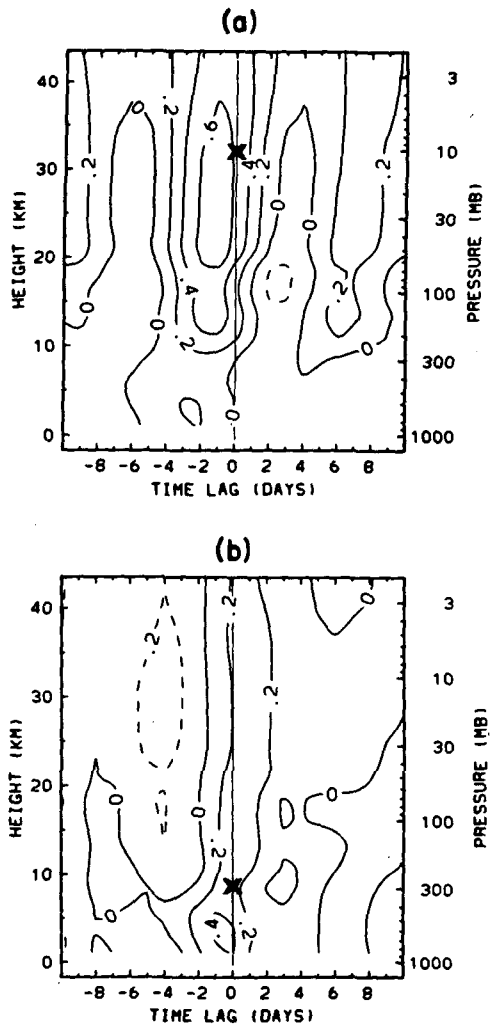

FIG. 7. As in Figs. 5a–b but for wave 2 cross-correlations.

downward movement subsequent to upper-level maxima is suggested in the cross-correlation patterns in Part I (see Figs. 5a, b of Part I).

c. *Composite analyses*

An average or composite analysis of upward propagating cases is made here to study the wave structure throughout a "typical" life cycle. The bases for choosing the particular cases in the composite were that each event be of large amplitude and separated in time from other wave growth episodes. Particular cases were scrutinized based on the energetic analyses just discussed, in addition to the wave amplitude plots in Fig. 13a–b. Here the k = 1–2 'amplitude' (the square root of the sum of the amplitudes squared of waves 1 and 2 individually) averaged over 45–65°S is plotted for several vertical levels from 500 to 5 mb. The amplitude at each pressure is weighted by $e^{-z/2H}$ and displaced by 100 gpm from the previous level, allowing vertical propagation to be traced by eye. Upper-level maxima can clearly be traced throughout all pressure levels, with a tilt in time indicative of upward propagation. However, not all maxima in the troposphere reach the stratosphere; a clear example is found near 12 July in Fig. 13a, which does not penetrate above 50 mb.

It is puzzling that some tropospheric planetary waves propagate into the stratosphere while others do not. One explanation is that the refractive characteristics of the zonal wind prevent vertical propagation in some cases while allowing it for others. To test this we calculate the refractive index $Q_{c,k}$ (Palmer, 1982) for the zonal flow corresponding to propagating and nonpropagating cases. Quasi-geostrophic wave theory predicts that EP flux (group velocity) vectors will flow along ridges of $Q_{c,k}$, in addition to being refracted towards larger values of $Q_{c,k}$ (Smith, 1983; Palmer, 1982). Figures 14a–b show contours of the zonal wind and refractive index $Q_{c,k}$ for propagating and nonpropagating cases centered on 12 and 19 July 1983 (the $Q_{c,k}$ calculations are made for k = 1 and c = 0 m s^{-1}; near identical results are found for k = 2 and c = 10 m s^{-1}). Superimposed on these figures are the EP flux or group velocity vectors averaged over these days.

Although near identical $Q_{c,k}$ contours are observed between these two periods, vertical propagation in the stratosphere is apparent over 18–20 July (Fig. 14b), while little is found for 11–13 July (Fig. 14a). The major difference between these examples is that the nonpropagating case (Fig. 14a) shows strong upward tropospheric EP vectors in low latitudes (30–40°S); the cross-correlation patterns in section 3 suggest that propagation into the stratosphere occurs primarily over the 45–65° latitude band, as observed in Fig. 14b. This is also consistent with the large $Q_{c,k}$ values in this latitude band in the lower stratosphere in Figs. 14a–b. Thus in this example it appears that the latitudinal region of tropospheric forcing is the factor determining

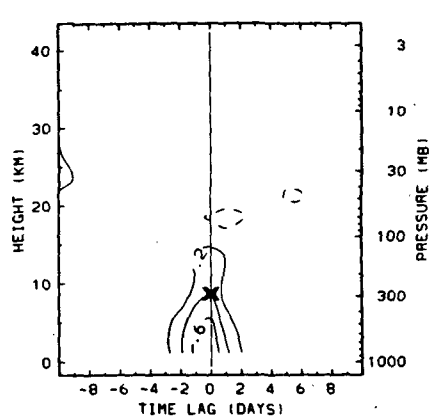

FIG. 8. As in Fig. 5a, but for wave 4 cross-correlations at 50°S, with a wave amplitude reference position at 300 mb. Zero contour lines have been omitted.

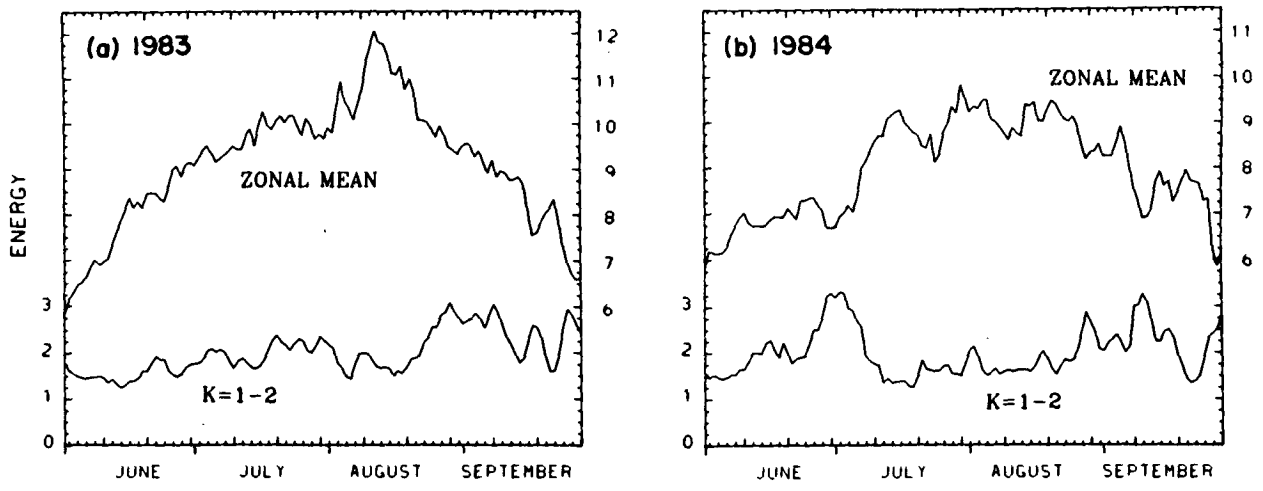

FIG. 9. Time variations in stratospheric (100–2 mb) zonal mean available potential plus kinetic energy for the zonal mean (top) and that for k = 1–2 (bottom). Units are 10^5 J m^{-2}. (a) 1983, (b) 1984.

propagation into the stratosphere, rather than time changes in the refractive properties of the zonal state. Similar calculations suggest that the polar night jet's poleward and downward seasonal progression is likely responsible for the late winter increase in stratospheric wave activity, as discussed in Mechoso et al. (1985) and Shiotani and Hirota (1985).

The five individual vertically propagating cases composited over these two winters are based primarily on Figs. 11a–b and 13a–b, and are indicated by the light lines superimposed in both figures. This composite was only done after noting that each case exhibits similar overall characteristics; the compositing is an attempt to characterize an average case, and remove some amount of noise. Note that a similar energetic life cycle is clearly observed for each of these cases, with peaks in the baroclinic term occurring prior to the energy maxima. Averages are made for k = 1–2 wave amplitude and EP flux vectors and divergence. These are displayed in Fig. 15 for 6 days centered on the day of tropospheric wave amplitude maximum (called composite day 0), determined from Figs. 13a–b. The stratospheric maximum occurs near composite day 4; cross-sections beyond day 3 are not shown because unrelated tropospheric maxima would be involved. Wave amplitudes in Fig. 15 are weighted by $e^{-z/2H}$ to remove the effect of density stratification.

The wave amplitude cross sections in Fig. 15 clearly show the upward wave propagation. The main tropospheric amplitude maximum is situated near 55°–60°S; enhanced wave amplitudes at low (30°–35°S) and high (70°–80°S) latitudes hint at secondary maxima. Such additional (out-of-phase) tropospheric maxima are clearly observed in Part I (see Figs. 6 and 12 of Part I). The stratospheric amplitude maximum in Fig. 15 is an extension of the main tropospheric peak near 55–60°S. Note that the tropospheric amplitude maximum decays rather quickly over days +1 → +3, whereas the stratospheric peak remains fairly constant. The disparate time scales of stratospheric versus tropospheric

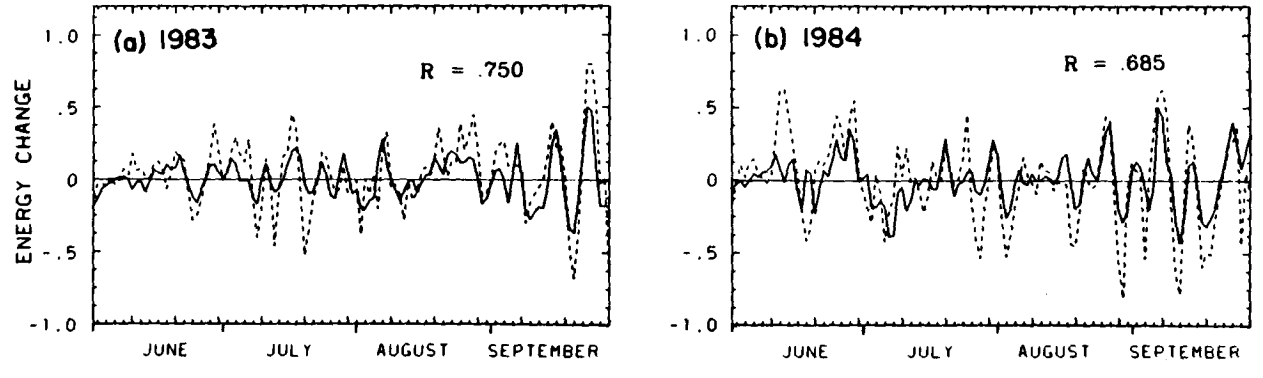

FIG. 10. Observed k = 1–2 total energy change (solid line) and that calculated by Eq. (4) (dashed line). The linear correlation (R) is also shown. Units are 10^5 J m^{-2}/day. (a) 1983, (b) 1984.

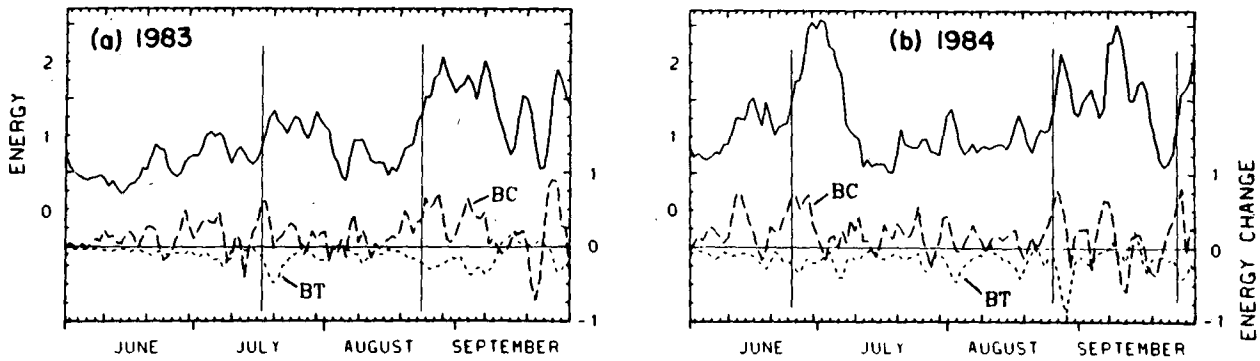

FIG. 11. Observed $k = 1$–2 wave energy (solid line), along with baroclinic (BC) and barotropic (BT) parts of wave–mean flow interaction term [Eq. (4)]. Units of energy are 10^5 J m^{-2}, while energy changes are in 10^5 J m^{-2}/day. (a) 1983, (b) 1984. Thin vertical lines denote composited vertically propagating cases.

planetary waves is clearly seen in Figs. 13a–b, and quantified in appendix A of Part I.

The composited EP flux diagrams in Fig. 15 show particularly strong upward wave propagation in the lower stratosphere over 50°–65°S for days −1 to +2. There is convergence of EP flux in the lower stratosphere (near 100 mb) over this time, whereas following day +1, the convergence is predominantly in the low to middle latitude upper stratosphere. The vertical arrow components are somewhat discontinuous near the tropopause for days 0 to +3; this agrees with the cross correlation patterns (Figs. 3–7) which suggested discontinuous F_Z across the tropopause. Upward EP flux vectors are observed in the high latitude lower troposphere (below 500 mb) throughout the composite, and some continuity into the lower stratosphere is observed for days −2 to 0. Following day 0 these low-level vectors converge near 500 mb; much of the wave activity which propagates into the stratosphere originates in the middle to high latitude *upper* troposphere, as signified by the divergent EP flux in this region. It is significant that a similar planetary wave EP flux divergence pattern in the upper troposphere is observed for the case study presented by Yamazaki and Mechoso (1985, their Fig. 9), the transient wave statistics of Hartmann et al. (1984, their Figs. 13 and 14), and the NH sudden warming study by O'Neill and Youngblut (1982, their Fig. 5a).

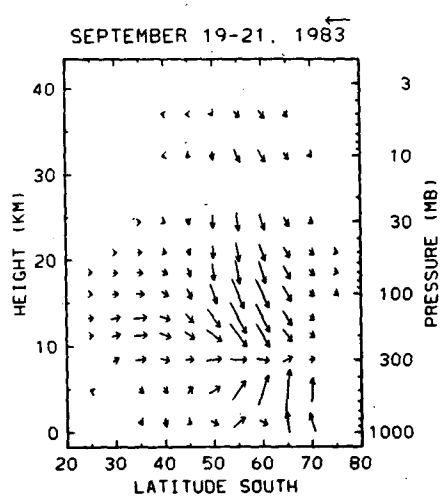

FIG. 12. EP flux vectors averaged over 19–21 September 1983, a period of intense baroclinic decay (see Fig. 11a). Such patterns frequently occur subsequent to stratospheric wave energy maxima. Note the strong equatorward heat flux (downward pointing arrows) in the lower stratosphere.

The horizontal component of the stratospheric EP vectors is observed to grow as the wave amplitude increases in the stratosphere, showing that barotropic processes become important. The familiar horizontal dipole pattern of wave forcing is observed throughout the entire time that wave amplitude is large in the stratosphere. The result of these barotropic interactions is a net transfer of energy from the waves to the zonal mean flow (see Figs. 11a–b).

Figure 16a shows an EP flux diagram averaged over the 7 days of Fig. 15, and Fig. 16b shows the observed zonal wind acceleration composited over the same times. By observing wind changes over a short time such as this (6 days), seasonal variations are minimized with respect to wave-induced changes. Zonal wind accelerations on the order of 1 m s^{-1} per day are observed in the middle to upper stratosphere. Figure 16c shows the composited zonal mean temperature changes, illustrating that these wave events tend to warm the polar upper stratosphere at a rate on the order of 1°K day^{-1}.

Some interesting time variations at 10 mb throughout the composite are shown in Fig. 17. Figure 17a shows the growth in wave amplitude, while Fig. 17b shows a qualitatively similar increase in quasi-geostrophic wave activity A (defined in Eq. 6). Because $\bar{q}_y$ becomes small and/or negative poleward of 70°S, calculated values of A show irregular behavior in this region, and are not shown. Note however that the wave potential enstrophy, $\frac{1}{2}\overline{q'^2}$, is also small poleward of 70°S, and most of the interesting variations are still observed in Fig. 17b.

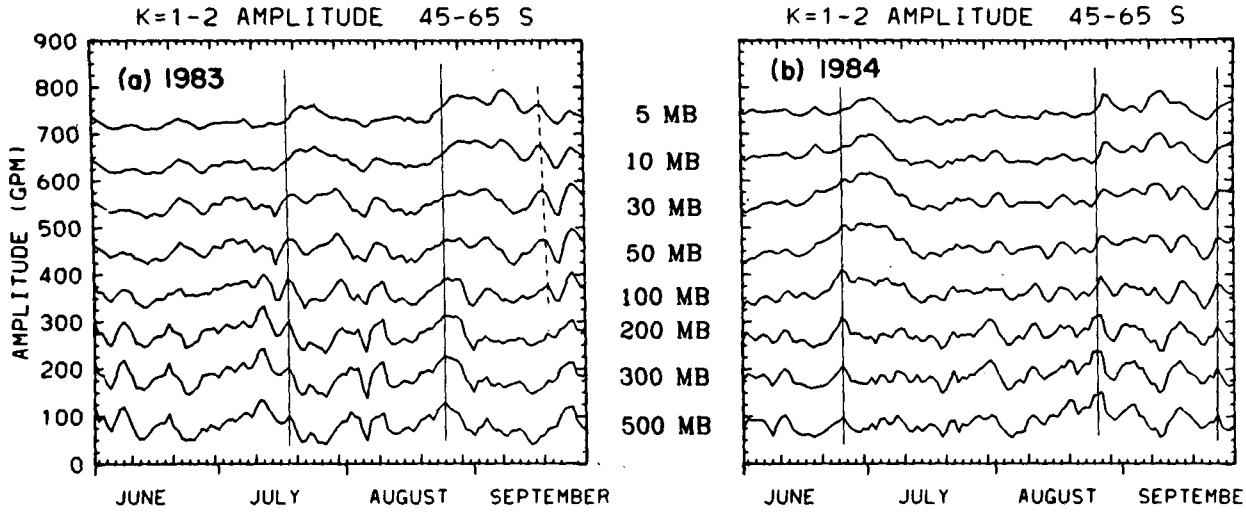

FIG. 13. Time variations of $k = 1$–2 amplitude (defined in text, gpm) averaged over 45°–65°S at the indicated pressure levels and weighted by $e^{-z/2H}$. Adjacent curves are displaced by 100 gpm, allowing vertical propagation to be traced by eye. (a) 1983, (b) 1984. Composited propagating cases indicated by thin vertical lines. Note the apparent downward propagating event near 20 September in (a), highlighted with dashed line; this corresponds to the time period in Fig. 12.

Figure 17c shows the quantity $-\partial A/\partial t$, calculated from the values of A in Fig. 17b. This quantity is interesting because linear theory predicts it to be proportional to the wave forcing term DF [see Eq. (5)]. Figure 17d displays the observed wave forcing for comparison. Negative values of $-\partial A/\partial t$ (growth of local wave activity) are observed over 35°–65°S for days −1 to 3, in good agreement with similar negative DF values at this time over 30°–55°S. Agreement is poor polewards of 60°S, where the wave driving is positive.

The agreement found in midlatitudes between $-\partial A/\partial t$ and DF in the composite analysis led to testing the correlation between $-\partial A/\partial t$ and DF at each point in the meridional plane [because Eq. (5) is valid locally]. Figure 18 shows this correlation during 1983. A surprising degree of correlation is observed throughout the midlatitude stratosphere (surprising because of the large number of derivatives used in the calculations); similar correlations are observed during 1984. Figure 19 shows time series of both at 10 mb averaged over 50°–60°S, illustrating the similar size variations in both quantities. These good correlations and similar size

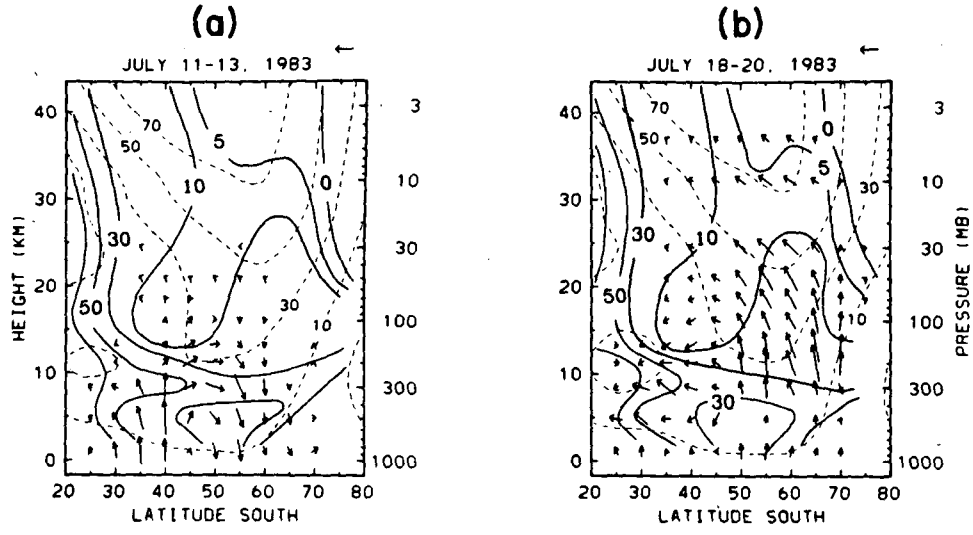

FIG. 14. (a) Contours of the zonal wind (dashed lines, units of m s^{-1}) and refractive index $Q_{c,k}$ (solid lines, units of 10^{-12} m^{-2}) averaged over 11–13 July 1983, along with the corresponding EP flux vectors averaged over the same period. (b) As in (a) but for 18–20 July 1983. Although the zonal wind and refractive index contours in (a) and (b) are nearly identical, case (b) shows vertical propagation in the stratosphere while little is seen in case (a).

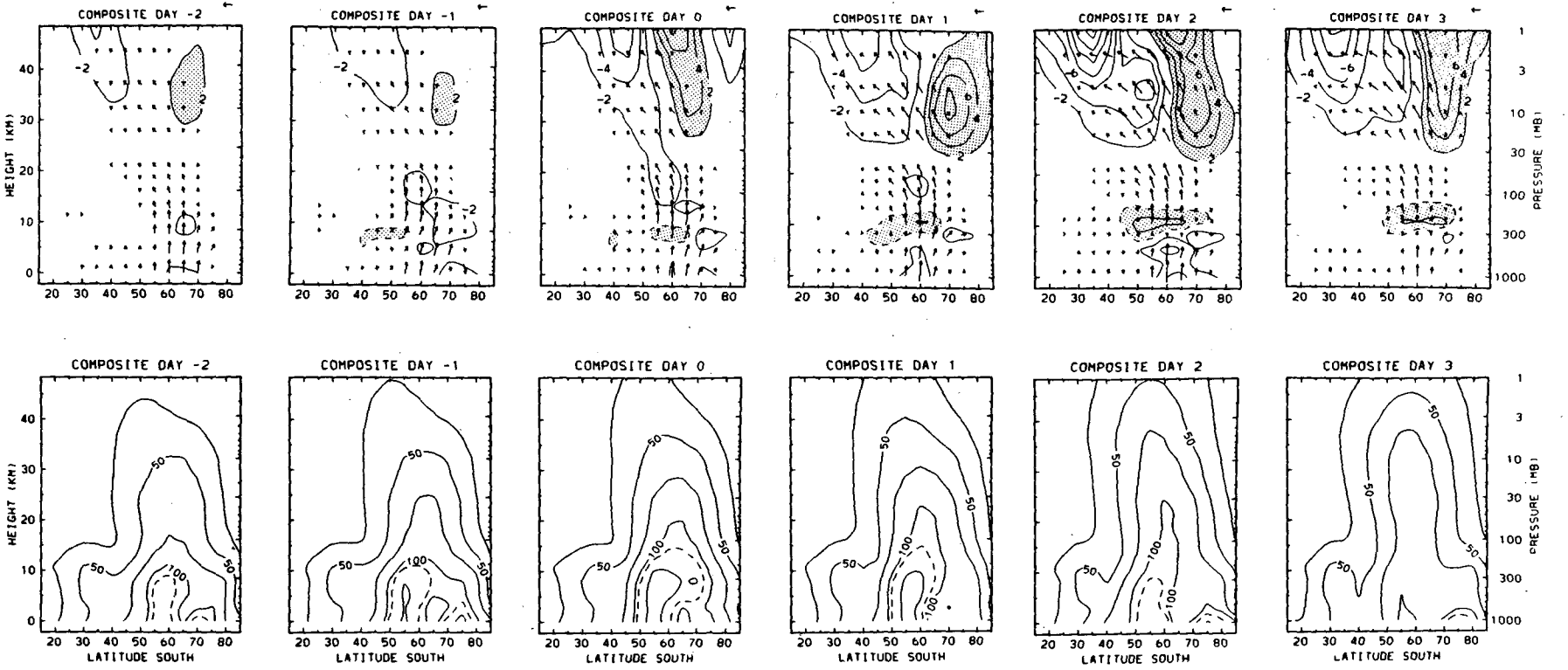

FIG. 15. EP flux diagrams (top) and wave amplitude weighted by $e^{-z/2H}$ (bottom, gpm) for the composited vertically propagating cases (see Figs. 11 and 13). Day 0 is the day of peak wave amplitude in the troposphere, determined from Fig. 13. The wave driving has a contour interval of 2 m s^{-1}/day, positive values are shaded, and the 0.5 contour below 100 mb is added as a dashed line. The 110 gpm contour is added as a dashed line in the lower figures to clarify the tropospheric structure.

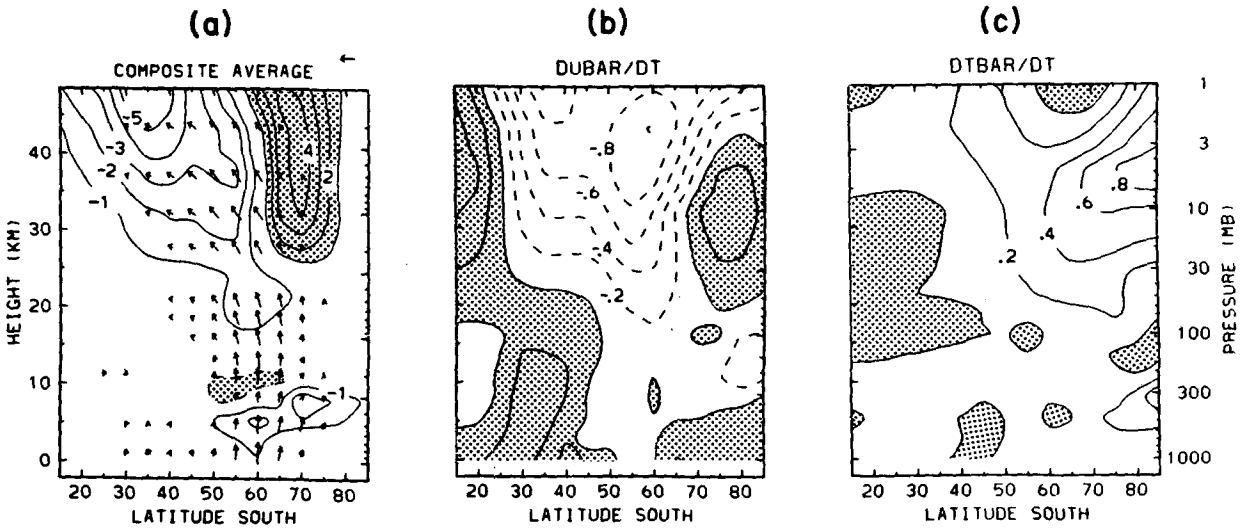

FIG. 16. (a) Composited 6-day average EP flux diagram (i.e., average of six days from Fig. 15); units of DF are m s^{-1}/day, with the 0.25 contour added as a dashed line below 100 mb. (b) Zonal mean accelerations composited over the same times, with contour interval of 0.2 m s^{-1} per day. (c) Composited zonal mean temperature changes, units of °K per day.

variations show that the local quasi-geostrophic wave activity is a valid conservable quantity in this region, and suggests that nonconservative effects are small. Poor correlations are found in both the low and high latitude stratosphere.

The appearance of the positive DF region near 70°S throughout the life cycle (and in long-term means, see Fig. 1 of Part I) is intriguing because linear theory predicts this to be a source region of wave activity [See Eq. (5) and discussion following]. However, it is clear from the energetic analyses (Figs. 11a–b) that vertical propagation alone is responsible for wave growth in the stratosphere, and that barotropic processes act to transfer energy from the waves to the mean flow, not vice-versa (as would an internal instability). As discussed in section 2, the use of linear winds in the stratosphere (as in this study) reduces the estimates of poleward momentum flux (compared to geostrophic values), resulting in a reduction by approximately a factor of two the high latitude stratospheric wave driving. Inclusion of the zonal mean wind shear terms in the EP flux divergence estimates (i.e., primitive equation calculations with the vertical velocity set to zero) reduces the magnitude of the high latitude wave driving by approximately 25%, although the positive values persist. The results of Boville (1987) suggest that inclusion of the vertical velocity term makes a relatively small difference in this region. Thus although this positive EP flux divergence region does not correspond to a local source of wave activity, it appears to be a resilient feature in these data, and its exact nature awaits explanation.

4. Discussion

Observations of the southern winter troposphere and stratosphere provide an opportunity to study planetary wave generation and propagation in an environment where the time-mean component is relatively small. The results of the analyses here have answered some questions, while pointing to aspects that need further explanation.

It has been known since the advent of satellite observations that waves 1 and 2 propagate zonally at different speeds in the SH winter stratosphere. The cross-correlation studies in Part I demonstrated that waves 1 and 2 also propagate energy vertically with different time scales, with wave 1 having a characteristic propagation time scale between middle troposphere and middle stratosphere on the order of 4 days, while wave 2 takes 1–2 days. In addition, waves 1 and 2 were found to have quite distinct structures in the meridional plane; most notably, wave 1 fluctuations are out-of-phase between troposphere and stratosphere, whereas those of wave 2 (and wave 3) are nearly in phase.

In spite of these differences in wave structure, the dynamics studied here reveal similar signatures for the wave 1 and wave 2 components; both the correlation analyses and wave–mean flow diagnostics reveal similar results. The largest difference appears to be the faster vertical propagation time scale of wave 2 processes. The observed dispersive behavior and similarity in dynamical structure is suggestive of wave packet behavior. Once a tropospheric long-wave pattern develops, the different zonal components propagate vertically in a similar manner, but with their own time scales. The overall 'event' time scale may thus depend on the zonal (and meridional) spectrum of the forcing. Such behavior is clearly seen in plots like Fig. 13a–b for each wave number; most events have components of both wave 1 and 2, although some are spectrally pure (such as the examples shown in Part I).

The life cycle of the planetary waves has been studied here by averaging over several clear life cycles observed

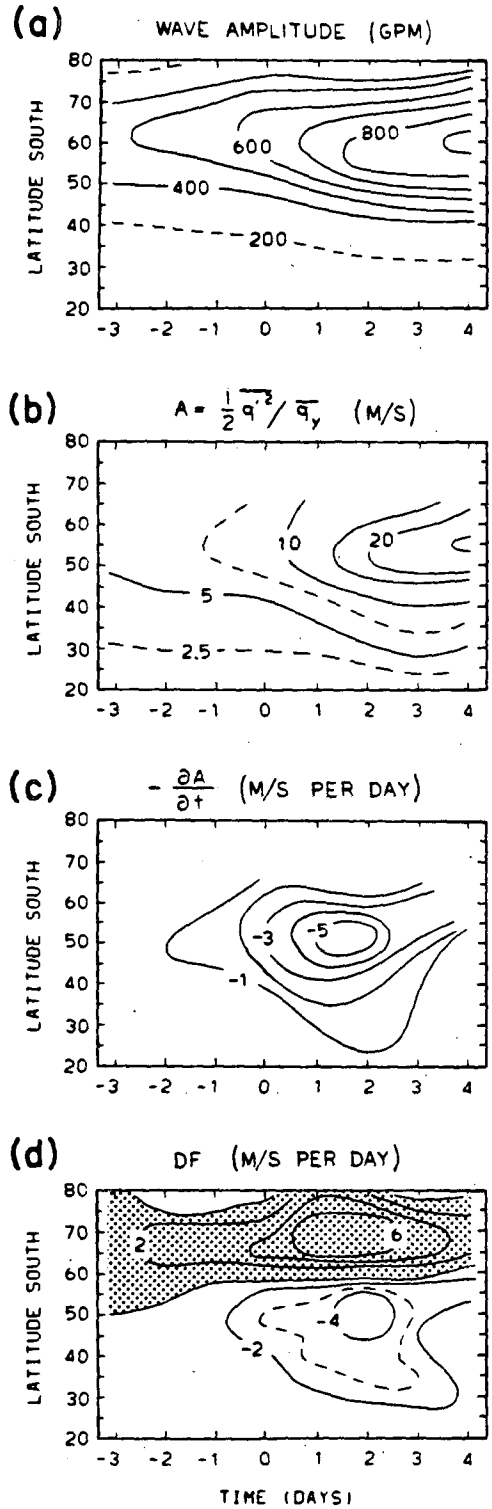

FIG. 17. Latitudinal time variations of composited cases at 10 mb. (a) Wave amplitude. (b) Wave activity A [Eq. (6)]. (c) Observed $-\partial A/\partial t$. (d) Wave-forcing DF.

during the 1983/84 winters. The EP flux diagnostics reveal strong vertical propagation from the lower stratosphere prior to upper-level amplitude maxima. The EP flux vectors show discontinuous vertical components across the tropopause region, particularly strong following the peak of wave amplitude in the troposphere, and a source of planetary wave activity is inferred in the middle to high latitude upper troposphere. This source region of wave activity is not related to an instability of the zonal mean flow because $\bar{q}_y$ is observed to be positive throughout this region, disparate with instability requirements. Rather, wave–wave interactions in the upper troposphere provide a likely source of this activity. High-latitude poleward heat flux is observed in low levels (below 500 mb) prior to and during wave growth, although little continuity into the stratosphere is observed following the time of peak wave amplitude in the troposphere. Thus, the sources of planetary wave growth in the troposphere may be linked to cooperative behavior between the long-wave spectral components of baroclinic waves and direct wave–wave coupling (which should maximize in the upper troposphere).

It is interesting to compare these observations with a recent modeling study of planetary waves generated by nonlinear interactions of medium-scale baroclinic waves (Young and Villere, 1985). They find poleward heat flux above the tropopause subsequent to the strongest wave-wave interactions, although it is an extension of that throughout the troposphere (not discontinuous as suggested here). Their computed planetary wave structure shows multiple latitudinal maxima in the troposphere as do the observations in Part I. This structure may also be a signature of linear planetary wave instability to the zonal mean flow (Hartmann, 1979), although the growth rates observed here are significantly larger than predicted for such a mechanism.

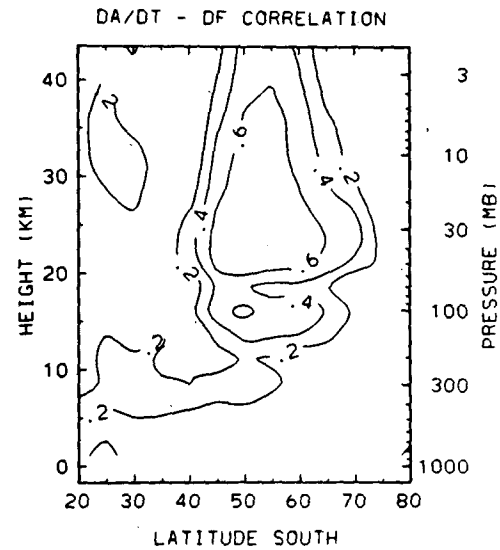

FIG. 18. Latitude–height cross section of the contemporaneous correlation coefficient between DF [Eq. (3)] and $\partial A/\partial t$ [Eq. (6)] for zonal waves 1–2 during 1983.

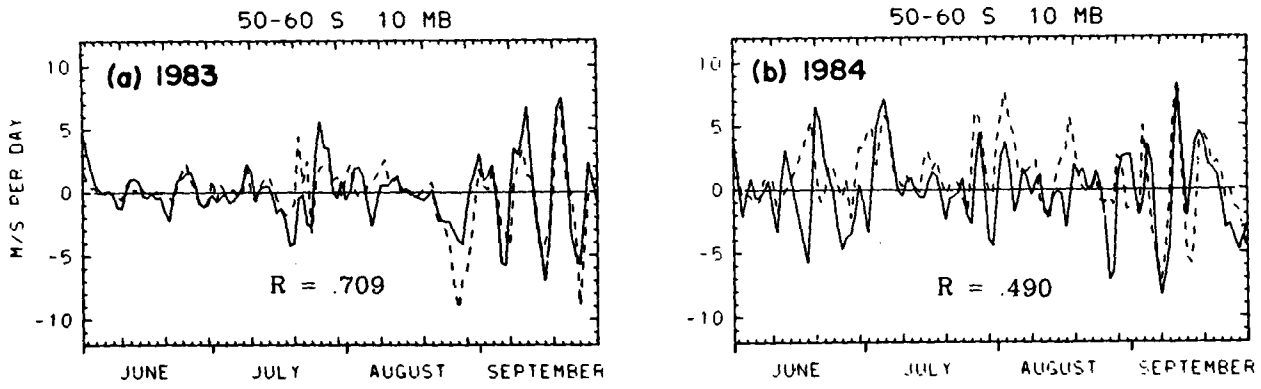

FIG. 19. Time series of the observed DF [Eq. (3), solid line] and $-\partial A/\partial t$ [Eq. (6), dashed line] at 10 mb, averaged over 50°–60°S for (a) 1983 and (b) 1984. The correlation coefficient (R) is shown for each series.

Analyses of the medium-scale wave behavior in the troposphere in connection with episodes of planetary wave generation studied here revealed no consistent behavior in terms of energetics (without detailed wave-wave calculations). Some cases showed medium-scale wave growth in tandem with the planetary waves, while other events showed an out-of-phase behavior. We suggest that further diagnostic analyses of wave-wave interactions are warranted.

The effect of the waves in the stratosphere is to warm the pole and decelerate the polar night jet. Episodic changes in the jet coincident with increased wave activity have been clearly observed by Hartmann et al. (1984) and Mechoso et al. (1985); this study quantifies these changes. The net decelerations to the jet core are generally on the order of 10 m s^{-1}, but occasionally larger events can occur (Al-Ajmi et al., 1985). Good agreement is found here between the observed wave driving and wave activity changes in the middle latitude stratosphere suggesting that nonconservative effects are small here on the time scale of wave growth-decay episodes.

Acknowledgments. Support for this work has been funded by the National Science Foundation under grants ATM-8305759 and ATM-8402901, and numerical computations were performed at the National Center for Atmospheric Research. Kevin Trenberth provided the ECMWF heat flux data. We thank the two anonymous reviewers for helpful comments on an earlier version of this manuscript.

REFERENCES

Al-Ajmi, D. N., R. S. Harwood and T. Miles, 1985: A sudden warming in the middle atmosphere of the Southern Hemisphere. *Quart. J. Roy. Meteor. Soc.*, **111**, 359–389.

Boville, B. A., 1987: The validity of the geostrophic approximation in the winter stratosphere and troposphere. *J. Atmos. Sci.*, **44**, 443–457.

Dunkerton, T., C.-P. Hsu and M. E. McIntyre, 1981: Some Eulerian and Lagrangian diagnostics for a model stratospheric warming. *J. Atmos. Sci.*, **38**, 819–843.

Hartmann, D. L., 1979: Baroclinic instability of realistic zonal mean states to planetary waves. *J. Atmos. Sci.*, **36**, 2336–2349.

——, C. R. Mechoso and K. Yamazaki, 1984: Observations of wave-mean flow interaction in the Southern Hemisphere. *J. Atmos. Sci.*, **41**, 351–362.

Mechoso, C. R., D. L. Hartmann and J. D. Farrara, 1985: Climatology and interannual variability of wave–mean flow interaction in the Southern Hemisphere. *J. Atmos. Sci.*, **42**, 2189–2206.

O'Neill, A., and C. E. Youngblut, 1982: Stratospheric warmings diagnosed using the transformed Eulerian-mean equations and the effect of the mean state on wave propagation. *J. Atmos. Sci.*, **39**, 1370–1386.

Palmer, T. N., 1982: Properties of the Eliassen–Palm flux for planetary scale motions. *J. Atmos. Sci.*, **39**, 992–997.

Plumb, R. A., 1983: A new look at the energy cycle. *J. Atmos. Sci.*, **40**, 1669–1688.

Randel, W. J., 1987: The evaluation of winds from geopotential height data in the stratosphere. *J. Atmos. Sci.*, **44**, 917–935.

——, 1987: A study of planetary waves in the southern winter troposphere and stratosphere. Part I: Wave Structure and Vertical Propagation. *J. Atmos. Sci.*, **44**, 917–935.

Robinson, W. A., 1986: The application of the quasi-geostrophic Eliassen–Palm flux to the analysis of stratospheric data. *J. Atmos. Sci.*, **43**, 1017–1023.

Shiotani, M., and I. Hirota, 1985: Planetary wave–mean flow interaction in the stratosphere: A comparison between Northern and Southern Hemispheres. *Quart. J. Roy. Meteor. Soc.*, **111**, 309–334.

Smith, A. K., 1983: Stationary waves in the winter stratosphere: Seasonal and interannual variability. *J. Atmos. Sci.*, **40**, 245–261.

van Loon, H., 1980: Transfer of sensible heat by transient eddies in the atmosphere of the Southern Hemisphere: An appraisal of the data before and during FGGE. *Mon. Wea. Rev.*, **108**, 1774–1781.

Yamazaki, K., and C. R. Mechoso, 1985: Observations of the final warming in the stratosphere of the Southern Hemisphere during 1979. *J. Atmos. Sci.*, **42**, 1198–1205.

Young, R. E., and G. L. Villere, 1985: Nonlinear forcing of planetary-scale waves by amplifying unstable baroclinic eddies generated in the troposphere. *J. Atmos. Sci.*, **42**, 1991–2006.